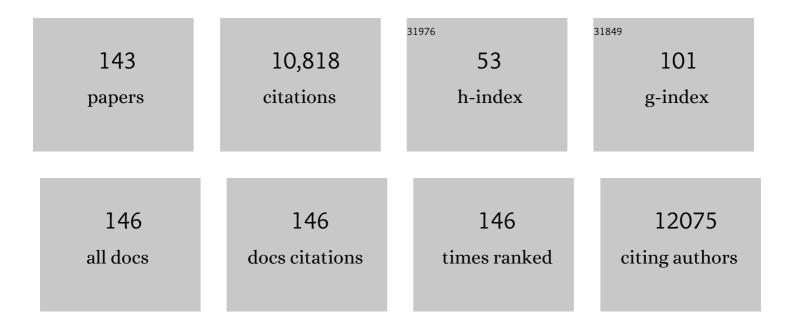
Sam M Webb

List of Publications by Year in descending order

Source: https://exaly.com/author-pdf/7749682/publications.pdf Version: 2024-02-01



SAM M WERR

#	Article	IF	CITATIONS
1	BIOGENIC MANGANESE OXIDES: Properties and Mechanisms of Formation. Annual Review of Earth and Planetary Sciences, 2004, 32, 287-328.	11.0	1,081
2	SIXPack a Graphical User Interface for XAS Analysis Using IFEFFIT. Physica Scripta, 2005, , 1011.	2.5	872
3	In Situ X-ray Absorption Spectroscopy Investigation of a Bifunctional Manganese Oxide Catalyst with High Activity for Electrochemical Water Oxidation and Oxygen Reduction. Journal of the American Chemical Society, 2013, 135, 8525-8534.	13.7	478
4	A Bacterium That Can Grow by Using Arsenic Instead of Phosphorus. Science, 2011, 332, 1163-1166.	12.6	422
5	Evidence for the presence of Mn(III) intermediates in the bacterial oxidation of Mn(II). Proceedings of the United States of America, 2005, 102, 5558-5563.	7.1	287
6	Structural characterization of biogenic Mn oxides produced in seawater by the marine bacillus sp. strain SG-1. American Mineralogist, 2005, 90, 1342-1357.	1.9	243
7	Biotic and abiotic products of Mn(II) oxidation by spores of the marineBacillus sp.strain SG-1. American Mineralogist, 2005, 90, 143-154.	1.9	237
8	Weathering of the Rio Blanco quartz diorite, Luquillo Mountains, Puerto Rico: Coupling oxidation, dissolution, and fracturing. Geochimica Et Cosmochimica Acta, 2008, 72, 4488-4507.	3.9	204
9	Enhanced Exopolymer Production and Chromium Stabilization in Pseudomonas putida Unsaturated Biofilms. Applied and Environmental Microbiology, 2006, 72, 1988-1996.	3.1	200
10	Coupled biotic–abiotic Mn(II) oxidation pathway mediates the formation and structural evolution of biogenic Mn oxides. Geochimica Et Cosmochimica Acta, 2011, 75, 6048-6063.	3.9	191
11	Manganese-oxidizing photosynthesis before the rise of cyanobacteria. Proceedings of the National Academy of Sciences of the United States of America, 2013, 110, 11238-11243.	7.1	189
12	Mn(II) oxidation by an ascomycete fungus is linked to superoxide production during asexual reproduction. Proceedings of the National Academy of Sciences of the United States of America, 2012, 109, 12621-12625.	7.1	178
13	Zinc sorption to biogenic hexagonal-birnessite particles within a hydrated bacterial biofilm. Geochimica Et Cosmochimica Acta, 2006, 70, 27-43.	3.9	177
14	Uranium Biomineralization as a Result of Bacterial Phosphatase Activity:  Insights from Bacterial Isolates from a Contaminated Subsurface. Environmental Science & Technology, 2007, 41, 5701-5707.	10.0	176
15	Photoreduction of iron oxyhydroxides in the presence of important atmospheric organic compounds. Environmental Science & Technology, 1993, 27, 2056-2062.	10.0	169
16	XAS Speciation of Arsenic in a Hyper-Accumulating Fern. Environmental Science & Technology, 2003, 37, 754-760.	10.0	168
17	Site Specific X-ray Anomalous Dispersion of the Geometrically Frustrated Kagomé Magnet, Herbertsmithite, ZnCu ₃ (OH) ₆ Cl ₂ . Journal of the American Chemical Society, 2010, 132, 16185-16190.	13.7	166
18	Arsenic Localization, Speciation, and Co-Occurrence with Iron on Rice (<i>Oryza sativa</i> L.) Roots Having Variable Fe Coatings. Environmental Science & Technology, 2010, 44, 8108-8113.	10.0	163

#	Article	IF	CITATIONS
19	Diversity of Mn oxides produced by Mn(II)-oxidizing fungi. Geochimica Et Cosmochimica Acta, 2011, 75, 2762-2776.	3.9	161
20	Uranium redox transition pathways in acetate-amended sediments. Proceedings of the National Academy of Sciences of the United States of America, 2013, 110, 4506-4511.	7.1	161
21	XANES Evidence for Oxidation of Cr(III) to Cr(VI) by Mn-Oxides in a Lateritic Regolith Developed on Serpentinized Ultramafic Rocks of New Caledonia. Environmental Science & Technology, 2009, 43, 7384-7390.	10.0	154
22	Manganese mineralogy and diagenesis in the sedimentary rock record. Geochimica Et Cosmochimica Acta, 2016, 173, 210-231.	3.9	150
23	Effects of Soluble Cadmium Salts Versus CdSe Quantum Dots on the Growth of Planktonic <i>Pseudomonas aeruginosa</i> . Environmental Science & Technology, 2009, 43, 2589-2594.	10.0	147
24	Trace Metals as Biomarkers for Eumelanin Pigment in the Fossil Record. Science, 2011, 333, 1622-1626.	12.6	147
25	Structure of Biogenic Uraninite Produced by <i>Shewanella oneidensis</i> Strain MR-1. Environmental Science & Technology, 2008, 42, 7898-7904.	10.0	119
26	Structural characterization of terrestrial microbial Mn oxides from Pinal Creek, AZ. Geochimica Et Cosmochimica Acta, 2009, 73, 889-910.	3.9	112
27	Uranium speciation and stability after reductive immobilization in aquifer sediments. Geochimica Et Cosmochimica Acta, 2011, 75, 6497-6510.	3.9	112
28	The MicroAnalysis Toolkit: X-ray Fluorescence Image Processing Software. AIP Conference Proceedings, 2011, , .	0.4	112
29	Microbiological Reduction of Sb(V) in Anoxic Freshwater Sediments. Environmental Science & Technology, 2014, 48, 218-226.	10.0	108
30	Efficient xylem transport and phloem remobilization of <scp>Z</scp> n in the hyperaccumulator plant species <i><scp>S</scp>edum alfredii</i> . New Phytologist, 2013, 198, 721-731.	7.3	106
31	Speciation Matters: Bioavailability of Silver and Silver Sulfide Nanoparticles to Alfalfa (<i>Medicago) Tj ETQq1 1</i>	0.784314 10.0	rgBT /Overlo
32	Pathogenic implications of distinct patterns of iron and zinc in chronic MS lesions. Acta Neuropathologica, 2017, 134, 45-64.	7.7	94
33	Nonreductive Biomineralization of Uranium(VI) Phosphate Via Microbial Phosphatase Activity in Anaerobic Conditions. Geomicrobiology Journal, 2009, 26, 431-441.	2.0	89
34	Spatial Imaging and Speciation of Lead in the Accumulator Plant <i>Sedum alfredii</i> by Microscopically Focused Synchrotron X-ray Investigation. Environmental Science & Technology, 2010, 44, 5920-5926.	10.0	89
35	A seafloor microbial biome hosted within incipient ferromanganese crusts. Nature Geoscience, 2009, 2, 872-876.	12.9	87
36	Enzymatic microbial Mn(II) oxidation and Mn biooxide production in the Guaymas Basin deep-sea hydrothermal plume. Geochimica Et Cosmochimica Acta, 2009, 73, 6517-6530.	3.9	85

#	Article	IF	CITATIONS
37	Determination of Uranyl Incorporation into Biogenic Manganese Oxides Using X-ray Absorption Spectroscopy and Scattering. Environmental Science & Technology, 2006, 40, 771-777.	10.0	81
38	Mercury Localization and Speciation in Plants Grown Hydroponically or in a Natural Environment. Environmental Science & Technology, 2013, 47, 3082-3090.	10.0	80
39	Defining the distribution of arsenic species and plant nutrients in rice (Oryza sativa L.) from the root to the grain. Geochimica Et Cosmochimica Acta, 2011, 75, 6655-6671.	3.9	75
40	Relating structure and composition with accessibility of a single catalyst particle using correlative 3-dimensional micro-spectroscopy. Nature Communications, 2016, 7, 12634.	12.8	74
41	Zinc and lead sequestration in an impacted wetland system. Journal of Environmental Management, 2003, 8, 103-112.	1.7	71
42	Characterization of manganese oxide precipitates from Appalachian coal mine drainage treatment systems. Applied Geochemistry, 2010, 25, 389-399.	3.0	71
43	Tracing Copperâ~'Thiomolybdate Complexes in a Prospective Treatment for Wilson's Disease. Biochemistry, 2009, 48, 891-897.	2.5	70
44	Neoarchean carbonate–associated sulfate records positive Δ ³³ S anomalies. Science, 2014, 346, 739-741.	12.6	70
45	Real-Time Manganese Phase Dynamics during Biological and Abiotic Manganese Oxide Reduction. Environmental Science & Technology, 2016, 50, 4248-4258.	10.0	69
46	Microscale Imaging and Identification of Fe Speciation and Distribution during Fluid–Mineral Reactions under Highly Reducing Conditions. Environmental Science & Technology, 2011, 45, 4468-4474.	10.0	65
47	The effect of pH and natural microbial phosphatase activity on the speciation of uranium in subsurface soils. Geochimica Et Cosmochimica Acta, 2011, 75, 5648-5663.	3.9	64
48	Microbial sulfate reduction and organic sulfur formation in sinking marine particles. Science, 2021, 371, 178-181.	12.6	64
49	Organic carbon burial during OAE2 driven by changes in the locus of organic matter sulfurization. Nature Communications, 2018, 9, 3409.	12.8	62
50	Chromium(<scp>iii</scp>) oxidation by biogenic manganese oxides with varying structural ripening. Environmental Sciences: Processes and Impacts, 2014, 16, 2127-2136.	3.5	61
51	High Rates of Sulfate Reduction in a Low-Sulfate Hot Spring Microbial Mat Are Driven by a Low Level of Diversity of Sulfate-Respiring Microorganisms. Applied and Environmental Microbiology, 2007, 73, 5218-5226.	3.1	59
52	Synchrotron X-ray analyses demonstrate phosphate-bound gadolinium in skin in nephrogenic systemic fibrosis. British Journal of Dermatology, 2010, 163, 1077-1081.	1.5	59
53	Quantifying Cr(VI) Production and Export from Serpentine Soil of the California Coast Range. Environmental Science & Technology, 2017, 51, 141-149.	10.0	58
54	The role of anaerobic respiration in the immobilization of uranium through biomineralization of phosphate minerals. Geochimica Et Cosmochimica Acta, 2013, 106, 344-363.	3.9	57

#	Article	IF	CITATIONS
55	Mineral Density Volume Gradients in Normal and Diseased Human Tissues. PLoS ONE, 2015, 10, e0121611.	2.5	57
56	Structural Influences of Sodium and Calcium Ions on the Biogenic Manganese Oxides Produced by the MarineBacillusSp., Strain SC-1. Geomicrobiology Journal, 2005, 22, 181-193.	2.0	56
57	Indirect Oxidation of Co(II) in the Presence of the Marine Mn(II)-Oxidizing Bacterium Bacillus sp. Strain SG-1. Applied and Environmental Microbiology, 2007, 73, 6905-6909.	3.1	56
58	Arsenic and chromium speciation in an urban contaminated soil. Chemosphere, 2012, 88, 1196-1201.	8.2	55
59	Sedimentary iron–phosphorus cycling under contrasting redox conditions in a eutrophic estuary. Chemical Geology, 2015, 392, 19-31.	3.3	55
60	Zinc Speciation in a Contaminated Aquatic Environment:Â Characterization of Environmental Particles by Analytical Electron Microscopy. Environmental Science & Technology, 2000, 34, 1926-1933.	10.0	52
61	The chemical, mechanical, and hydrological evolution of weathering granitoid. Journal of Geophysical Research F: Earth Surface, 2016, 121, 1410-1435.	2.8	49
62	Geochemical Weathering Increases Lead Bioaccessibility in Semi-Arid Mine Tailings. Environmental Science & Technology, 2012, 46, 5834-5841.	10.0	48
63	Determination of photochemically available iron in ambient aerosols. Journal of Geophysical Research, 1996, 101, 14441-14449.	3.3	46
64	The plastic nature of the human bone–periodontal ligament–tooth fibrous joint. Bone, 2013, 57, 455-467.	2.9	44
65	Uranium(VI) Interactions with Mackinawite in the Presence and Absence of Bicarbonate and Oxygen. Environmental Science & Technology, 2013, 47, 7357-7364.	10.0	44
66	Multiscale Speciation of U and Pu at Chernobyl, Hanford, Los Alamos, McGuire AFB, Mayak, and Rocky Flats. Environmental Science & Technology, 2015, 49, 6474-6484.	10.0	43
67	Spatial imaging of Zn and other elements in Huanglongbing-affected grapefruit by synchrotron-based micro X-ray fluorescence investigation. Journal of Experimental Botany, 2014, 65, 953-964.	4.8	42
68	Reexamination of 2.5-Ga "whiff―of oxygen interval points to anoxic ocean before GOE. Science Advances, 2022, 8, eabj7190.	10.3	42
69	Distributed microbially- and chemically-mediated redox processes controlling arsenic dynamics within Mn-/Fe-oxide constructed aggregates. Geochimica Et Cosmochimica Acta, 2013, 104, 29-41.	3.9	41
70	(Micro)spectroscopic Analyses of Particle Size Dependence on Arsenic Distribution and Speciation in Mine Wastes. Environmental Science & Technology, 2013, 47, 8164-8171.	10.0	40
71	Redox Fluctuations and Organic Complexation Govern Uranium Redistribution from U(IV)-Phosphate Minerals in a Mining-Polluted Wetland Soil, Brittany, France. Environmental Science & Technology, 2018, 52, 13099-13109.	10.0	40
72	Melanin Concentration Gradients in Modern and Fossil Feathers. PLoS ONE, 2013, 8, e59451.	2.5	39

#	Article	IF	CITATIONS
73	Discontinuities in the human bone–PDL–cementum complex. Biomaterials, 2011, 32, 7106-7117.	11.4	35
74	Leaf metallome preserved over 50 million years. Metallomics, 2014, 6, 774-782.	2.4	35
75	Tissue-specific geometry and chemistry of modern and fossilized melanosomes reveal internal anatomy of extinct vertebrates. Proceedings of the National Academy of Sciences of the United States of America, 2019, 116, 17880-17889.	7.1	32
76	Quick X-ray absorption spectroscopy for determining metal speciation in environmental samples. Journal of Synchrotron Radiation, 2001, 8, 928-930.	2.4	31
77	From lapis lazuli to ultramarine blue: investigating Cennino Cennini's recipe using sulfur K-edge XANES. Pure and Applied Chemistry, 2018, 90, 463-475.	1.9	31
78	Insights Into the Mineralogy and Surface Chemistry of Extracellular Biogenic SO Globules Produced by Chlorobaculum tepidum. Frontiers in Microbiology, 2019, 10, 271.	3.5	29
79	Biogenesis of zinc storage granules in <i>Drosophila melanogaster</i> . Journal of Experimental Biology, 2018, 221, .	1.7	28
80	Sulfur isotope fractionation between aqueous and carbonate-associated sulfate in abiotic calcite and aragonite. Geochimica Et Cosmochimica Acta, 2020, 280, 317-339.	3.9	28
81	Sulfur K-edge XANES of lazurite: Toward determining the provenance of lapis lazuli. Microchemical Journal, 2016, 125, 299-307.	4.5	26
82	Biomineralization of U(VI) phosphate promoted by microbially-mediated phytate hydrolysis in contaminated soils. Geochimica Et Cosmochimica Acta, 2017, 197, 27-42.	3.9	26
83	The Interaction of Bromide Ions with Graphitic Materials. Advanced Materials, 2009, 21, 102-106.	21.0	24
84	Dopant site selectivity in BaCe0.85M0.15O3-δ by extended x-ray absorption fine structure. Journal of Applied Physics, 2005, 97, 054101.	2.5	23
85	Response to Comments on "A Bacterium That Can Grow Using Arsenic Instead of Phosphorus― Science, 2011, 332, 1149-1149.	12.6	23
86	Depositional and diagenetic constraints on the abundance and spatial variability of carbonate-associated sulfate. Chemical Geology, 2019, 523, 59-72.	3.3	23
87	Iron Heterogeneity in Early Active Multiple Sclerosis Lesions. Annals of Neurology, 2021, 89, 498-510.	5.3	22
88	Cold crucible induction melter test for crystalline ceramic waste form fabrication: A feasibility assessment. Journal of Nuclear Materials, 2017, 486, 283-297.	2.7	21
89	EXAFS, XANES and In-Situ SRXRD Characterization of Biogenic Manganese Oxides Produced in Sea Water. Physica Scripta, 2005, , 888.	2.5	20
90	Arsenolipids in Cultured Picocystis Strain ML and Their Occurrence in Biota and Sediment from Mono Lake, California. Life, 2020, 10, 93.	2.4	20

#	Article	IF	CITATIONS
91	Changes in Zinc Speciation with Mine Tailings Acidification in a Semiarid Weathering Environment. Environmental Science & Technology, 2011, 45, 7166-7172.	10.0	19
92	A new synchrotron rapid-scanning X-ray fluorescence (SRS-XRF) imaging station at SSRL beamline 6-2. Journal of Synchrotron Radiation, 2018, 25, 1565-1573.	2.4	19
93	Sample preparation with sucrose cryoprotection dramatically alters Zn distribution in the rodent hippocampus, as revealed by elemental mapping. Journal of Analytical Atomic Spectrometry, 2020, 35, 2498-2508.	3.0	19
94	An ecophysiological explanation for manganese enrichment in rock varnish. Proceedings of the National Academy of Sciences of the United States of America, 2021, 118, .	7.1	19
95	X-ray fluorescence microscopy methods for biological tissues. Metallomics, 2022, 14, .	2.4	19
96	Efficient phloem remobilization of Zn protects apple trees during the early stages of Zn deficiency. Plant, Cell and Environment, 2019, 42, 3167-3181.	5.7	18
97	Microbial- and thiosulfate-mediated dissolution of mercury sulfide minerals and transformation to gaseous mercury. Frontiers in Microbiology, 2015, 6, 596.	3.5	17
98	Micro x-ray absorption spectroscopic analysis of arsenic localization and biotransformation in Chironomus riparius Meigen (Diptera: Chironomidae) and Culex tarsalis Coquillett (Culicidae). Environmental Pollution, 2013, 180, 78-83.	7.5	16
99	Strain-guided mineralization in the bone–PDL–cementum complex of a rat periodontium. Bone Reports, 2015, 3, 20-31.	0.4	16
100	Fate of cobalt and nickel in mackinawite during diagenetic pyrite formation. American Mineralogist, 2019, 104, 917-928.	1.9	16
101	Synchrotron X-ray absorption spectroscopy of melanosomes in vertebrates and cephalopods: implications for the affinity of <i>Tullimonstrum</i> . Proceedings of the Royal Society B: Biological Sciences, 2019, 286, 20191649.	2.6	16
102	Imaging of stroke: a comparison between X-ray fluorescence and magnetic resonance imaging methods. Magnetic Resonance Imaging, 2012, 30, 1416-1423.	1.8	15
103	Brine film thicknesses on mica surfaces under geologic CO ₂ sequestration conditions and controlled capillary pressures. Water Resources Research, 2013, 49, 5071-5076.	4.2	15
104	Deletion of Phytochelatin Synthase Modulates the Metal Accumulation Pattern of Cadmium Exposed C. elegans. International Journal of Molecular Sciences, 2016, 17, 257.	4.1	15
105	Chemical and Isotopic Evidence for Organic Matter Sulfurization in Redox Gradients Around Mangrove Roots. Frontiers in Earth Science, 2019, 7, .	1.8	15
106	An EXAFS study of zinc coordination in microbial cells. Journal of Synchrotron Radiation, 2001, 8, 943-945.	2.4	14
107	Coupled X-ray Fluorescence and X-ray Absorption Spectroscopy for Microscale Imaging and Identification of Sulfur Species within Tissues and Skeletons of Scleractinian Corals. Analytical Chemistry, 2018, 90, 12559-12566.	6.5	14
108	XAS Study of a Metal-Induced Phase Transition by a Microbial Surfactant. Langmuir, 2008, 24, 4999-5002.	3.5	13

#	Article	IF	CITATIONS
109	Evidence for the Root-Uptake of Arsenite at Lateral Root Junctions and Root Apices in Rice (Oryza) Tj ETQq1 1 0.	784314 rgE 1.0	3T_/Overloch
110	Seasonal Zinc Storage and a Strategy for Its Use in Buds of Fruit Trees. Plant Physiology, 2020, 183, 1200-1212.	4.8	12
111	Comparison of EXAFS foil spectra from around the world. Journal of Physics: Conference Series, 2009, 190, 012032.	0.4	11
112	Fe-bearing phases in modern lacustrine microbialites from Mexico. Geochimica Et Cosmochimica Acta, 2019, 253, 201-230.	3.9	11
113	Brachiopod δ34SCAS microanalyses indicate a dynamic, climate-influenced Permo-Carboniferous sulfur cycle. Earth and Planetary Science Letters, 2020, 546, 116428.	4.4	11
114	Zinc Speciation in Contaminated Sediments: Quantitative Determination of Zinc Coordination by X-ray Absorption Spectroscopy. Aquatic Geochemistry, 2015, 21, 295-312.	1.3	10
115	Insights into the Interconnection of the Electrodes and Electrolyte Species in Lithium–Sulfur Batteries Using Spatially Resolved <i>Operando</i> X-ray Absorption Spectroscopy and X-ray Fluorescence Mapping. Journal of Physical Chemistry C, 2018, 122, 5303-5316.	3.1	10
116	The source of sulfate in brachiopod calcite: Insights from μ-XRF imaging and XANES spectroscopy. Chemical Geology, 2019, 529, 119328.	3.3	10
117	Changing chemistry of particulate manganese in the near- and far-field hydrothermal plumes from 15ŰS East Pacific Rise and its influence on metal scavenging. Geochimica Et Cosmochimica Acta, 2021, 300, 95-118.	3.9	10
118	Rapid, Concurrent Formation of Organic Sulfur and Iron Sulfides During Experimental Sulfurization of Sinking Marine Particles. Global Biogeochemical Cycles, 2021, 35, e2021GB007062.	4.9	10
119	Periphyton and abiotic factors influencing arsenic speciation in aquatic environments. Environmental Toxicology and Chemistry, 2018, 37, 903-913.	4.3	9
120	Robust framework and software implementation for fast speciation mapping. Journal of Synchrotron Radiation, 2020, 27, 1049-1058.	2.4	9
121	Hierarchical biota-level and taxonomic controls on the chemistry of fossil melanosomes revealed using synchrotron X-ray fluorescence. Scientific Reports, 2020, 10, 8970.	3.3	9
122	Organic sulfur fluxes and geomorphic control of sulfur isotope ratios in rivers. Earth and Planetary Science Letters, 2021, 562, 116838.	4.4	9
123	Iron mineralogy and redox conditions during deposition of the mid-Proterozoic Appekunny Formation, Belt Supergroup, Glacier National Park. Special Paper of the Geological Society of America, 2016, , 221-242.	0.5	8
124	Reply to Jones and Crowe: Correcting mistaken views of sedimentary geology, Mn-oxidation rates, and molecular clocks. Proceedings of the National Academy of Sciences of the United States of America, 2013, 110, E4119-20.	7.1	8
125	Nutrient and pollutant metals within earthworm residues are immobilized in soil during decomposition. Soil Biology and Biochemistry, 2016, 101, 217-225.	8.8	8
126	Manganese oxides in Martian meteorites Northwest Africa (NWA) 7034 and 7533. Icarus, 2021, 364, 114471.	2.5	8

#	Article	IF	CITATIONS
127	Imaging translocation and transformation of bioavailable selenium by Stanleya pinnata with X-ray microscopy. Analytical and Bioanalytical Chemistry, 2012, 404, 1277-1285.	3.7	7
128	Elastic discontinuity due to ectopic calcification in a human fibrous joint. Acta Biomaterialia, 2013, 9, 4787-4795.	8.3	7
129	Constraints on Precipitation of the Ferrous Arsenite Solid H ₇ Fe ₄ (AsO ₃) ₅ . Journal of Environmental Quality, 2014, 43, 947-954.	2.0	7
130	Copper Speciation in Variably Toxic Sediments at the Ely Copper Mine, Vermont, United States. Environmental Science & Technology, 2016, 50, 1126-1136.	10.0	7
131	Midâ€Proterozoic Ferruginous Conditions Reflect Postdepositional Processes. Geophysical Research Letters, 2019, 46, 3114-3123.	4.0	7
132	Investigation of the effect of taurine supplementation on muscle taurine content in the mdx mouse model of Duchenne muscular dystrophy using chemically specific synchrotron imaging. Analyst, The, 2020, 145, 7242-7251.	3.5	7
133	The narwhal (<i>Monodon monoceros</i>) cementum–dentin junction: A functionally graded biointerphase. Proceedings of the Institution of Mechanical Engineers, Part H: Journal of Engineering in Medicine, 2014, 228, 754-767.	1.8	6
134	Reinforcement Learning for Adaptive Illumination with X-rays. , 2020, , .		6
135	Electrochemically induced metal- <i>vs.</i> ligand-based redox changes in mackinawite: identification of a Fe ³⁺ - and polysulfide-containing intermediate. Dalton Transactions, 2021, 50, 11763-11774.	3.3	6
136	Fate of Neptunium in an Anaerobic, Ethanogenic Microcosm. Materials Research Society Symposia Proceedings, 1999, 556, 1141.	0.1	5
137	Photons, Folios, and Fossils: The X-ray Imaging and Spectroscopy Program of Ancient Materials at SSRL. Synchrotron Radiation News, 2019, 32, 22-28.	0.8	4
138	Deposition of sulfate aerosols with positive Δ33S in the Neoarchean. Geochimica Et Cosmochimica Acta, 2020, 285, 1-20.	3.9	4
139	Trace Impurities Identified as Forensic Signatures in CMX-5 Fuel Pellets Using X-ray Spectroscopic Techniques. Analytical Chemistry, 2022, 94, 7084-7091.	6.5	4
140	Molecular genetic and biochemical characterization of a putative family of zinc metalloproteins in Caenorhabditis elegans. Metallomics, 2018, 10, 1814-1823.	2.4	2
141	Synchrotron xâ€ray fluorescence analysis reveals diagenetic alteration of fossil melanosome trace metal chemistry. Palaeontology, 2021, 64, 63-73.	2.2	2
142	X-ray Fluorescence Spectroscopy of Picrolite Raw Material on Cyprus. Heritage, 2022, 5, 664-677.	1.9	1
143	MP19-17 SPATIAL DISTRIBUTION AND CONCENTRATION OF ELEMENTS WITHIN LIESEGANG-LIKE RINGS IN APATITE-BASED KIDNEY STONES. Journal of Urology, 2016, 195, .	0.4	0